Thermodynamic interpolation for the simulation of two-phase flow of non-ideal mixtures

S. Brown [a,1], L.D. Peristeras [b], S. Martynov [a], R.T.J. Porter [a], H. Mahgerefteh [a,*], Ilias K. Nikolaidis [b], Georgios C. Boulougouris [b,c], Dimitrios M. Tsangaris [b], Ioannis G. Economou [b,d]

[a] Department of Chemical Engineering, University College of London, London WC1E7JE, UK
[b] National Center for Scientific Research "Demokritos", Institute of Nanoscience and Nanotechnology, Molecular Thermodynamics and Modelling of Materials Laboratory, Agia Paraskevi, Attikis GR-153 10, Greece
[c] Department of Molecular Biology and Genetics, Democritus University, 68100 Alexandroupolis, Greece
[d] Texas A&M University at Qatar, Chemical Engineering Program, 23874 Doha, Qatar

ARTICLE INFO

ABSTRACT

This paper describes the development and application of a technique for the rapid interpolation of thermodynamic properties of mixtures for the purposes of simulating two-phase flow. The technique is based on adaptive inverse interpolation and can be applied to any Equation of State and multicomponent mixture. Following analysis of its accuracy, the method is coupled with a two-phase flow model, based on the homogeneous equilibrium mixture assumption, and applied to the simulation of flows of carbon dioxide (CO_2) rich mixtures. This coupled flow model is used to simulate the experimental decompression of binary and quinternary mixtures. It is found that the predictions are in good agreement with the experimental data and that the interpolation approach provides a flexible, robust means of obtaining thermodynamic properties for use in flow models.

© 2016 Elsevier Ltd. All rights reserved.

1. Introduction

The modelling of compressible two-phase or flashing flows is commonplace in a wide range of areas in engineering. For example, cavitation in automotive fuel injection systems (Martynov, 2006), flash boiling of water during loss-of-coolant accidents in nuclear reactors (Blinkov et al., 1993) and liquid boiling and expansion in refrigeration systems and heat pumps (Simões-Moreira and Bullard, 2003). Whilst various approaches are available to model the dynamics of two-phase flow, the accuracy of simulations for flashing two-phase flows to a large extent depends on the accuracy of the physical properties data in use. This particularly applies to multicomponent mixtures, which are commonly found as working fluids in the above systems.

In practice, complex mathematical formulas known as Equations of State (EoS), are used to provide the thermodynamic properties for both vapour and liquid phases. As a result, a prac-

tical problem arises when pressure explicit EoS are coupled with flow models. In these EoS, the thermodynamic properties are predicted as a function of pressure, temperature and composition while phase equilibria, at a given system pressure and temperature (*P-T*), is determined using a variety of isothermal 'flash' algorithms (Michelsen, 1982a,b). This formulation contrasts with the fluid-dynamics models, where the conservation laws governing are naturally posed in terms of density and internal energy (ρ-e). To overcome this problem, one possible solution is to use the so-called isochoric-isoenergetic flash (Castier, 2009; Michelsen, 1999). However, existing isochoric-isoenergetic flash algorithms are neither robust nor computationally efficient in the context of flow simulation because they either rely on an internal iterative loop over the *P-T* variables (Michelsen, 1999; Saha and Carroll, 1997) or on the direct minimisation of total entropy (Castier, 2009; Munkejord and Hammer, 2015).

The problem of computational inefficiency is exacerbated by the complexity of modern EoS. In the oil and gas industry, fluid flow simulators almost exclusively use cubic EoS (such as Soave-Redlich-Kwong, Peng-Robinson, etc., Zaydullin et al., 2014). Cubic EoS can be solved relatively at low computational cost; however, the higher order EoS developed in the last two decades provide

improved accuracy in physical property estimations, though this is at slightly higher computational cost. For example, for the case of CO_2 and its mixtures, high accuracy is provided by the Statistical Associating Fluid Theory (SAFT) EoS (Diamantonis and Economou, 2011) or by the "reference" EoS (Span and Wagner, 1996) and both EoS have a large number of relatively complex terms. As a result, application of these EoS to flow simulations not only increases the computational cost, but also the susceptibility to numerical instabilities in the underlying isothermal flash algorithms.

This is a particular problem in the simulation of flows associated with Carbon Capture and Storage (CCS), where the CO_2 stream may contain a number of impurities and vary in composition (Porter et al., 2015). Indeed, it is well established that the presence of these impurities has important impacts on many aspects where the modelling of two-phase flow is relevant, including ductile fracture (Mahgerefteh et al., 2012a) and the release rate in the case of loss of containment (Brown et al., 2013).

Previous work to address this issue has focused on producing tables of thermodynamic properties from isenthalpic or isentropic flash calculations (Mahgerefteh et al., 2006), which are facilitated by changing the variables with which the flow is resolved; however, this means that alternative numerical techniques must be applied to the fluid flow equations and that conservation of mass, momentum and energy is not ensured. Similarly, isothermal tables to replace the isothermal flash in the iterative loop described above have been widely applied (for example Andresen, 2009; Zaydullin et al., 2014); in particular, Zaydullin et al. (2014) extended the compositional space adaptive tabulation (CSAT) technique of Iranshahr et al. (2010) and applied it to compositional and thermal reservoir simulations of multicomponent multiphase systems. In this case, the generalised negative flash approach (Iranshahr et al., 2010) was used to first establish and then extend the set of tie-simplexes for the CSAT procedure. These tie-simplexes were then used to look up, for a particular pressure and temperature, the phase state of the mixture. Dumbser et al. (2013) presented a method of building an interpolating function in terms of density and internal energy using adaptive mesh refinement for a single component fluid; however, this relied on the ability to calculate isochoric-isoenergetic flashes which cannot be done efficiently for mixtures.

In this work a robust technique for efficiently performing isochoric-isoenergetic flashes, for the purposes of two-phase flow calculations, is presented. The technique is based on adaptive inverse interpolation and can be applied independently of the EoS and the specific mixture under consideration. The technique is intended for the application of the complex, computationally heavy EoS that are required for the accurate prediction of the thermodynamic properties and phase equilibria of CO_2 mixtures. For this study, the Perturbed Chain-SAFT (PC-SAFT) is selected for this purpose (Gross and Sadowski, 2001); however, any other EoS can be used. PC-SAFT is an accurate EoS rooted in statistical mechanics that has gained significant interest by oil and gas and chemical industries in recent years for the calculation of thermodynamic properties. This is the first attempt, to our knowledge, to use PC-SAFT for compressible fluid flow simulations, although it has been applied to multiphase flows in other contexts such as within hydrocarbon reservoirs (see for example Mohebbinia, 2013; Yan et al., 2015). The new method is then coupled with a two-phase flow model based on the homogeneous equilibrium mixture assumption (Brown et al., 2015a; Mahgerefteh et al., 2012b) and applied to the simulation of CCS relevant two-phase flows.

This paper is structured as follows: Section 2 firstly presents the fluid flow model applied in this study (Section 2.1) followed by a description of the interpolation scheme developed based on well-established and widely adopted techniques (Section 2.2). The section ends with an overview of the PC-SAFT EoS used in this work.

Section 3 provides an analysis of the interpolation technique's consistency with the EoS (Section 3.1). Next, the method is coupled with the two-phase flow model and a number of tests are performed to establish the robustness and computational efficiency of the method in the presence of rapid transients (Section 3.2). This coupled flow model is then used to predict the decompression of binary and quinternary mixtures and the results are compared against experimental data, which in the case of the binary data is previously unpublished (Section 3.3). Conclusions and suggestions for future work are discussed in Section 4.

2. Methodology

2.1. The homogeneous equilibrium model (HEM) flow model

The model applied in this study is based on the assumptions of one-dimensional, unsteady flow and, in the case of two-phase flow, thermodynamic and mechanical equilibrium, i.e. a single temperature, pressure and velocity, between the saturated vapour and liquid phases. In this case the respective continuity, momentum, and energy conservation equations are given by (see for example Zucrow and Hoffman, 1975):

$$\frac{\partial \rho}{\partial t} + \frac{\partial \rho u}{\partial z} = 0 \tag{1}$$

$$\frac{\partial \rho u}{\partial t} + \frac{\partial \rho u^2 + P}{\partial z} = -2f_w \frac{\rho u^2}{D_p} \tag{2}$$

$$\frac{\partial E}{\partial t} + \frac{\partial u(E+P)}{\partial z} = -2f_w \frac{\rho u^3}{D_p} \tag{3}$$

where ρ, u, P are respectively the mixture density, velocity and pressure, which are functions of time, t, and spatial coordinate, z; D_p and f_w, are the pipeline diameter and Fanning friction factor, calculated using Chen's correlation (Chen, 1979), and E is the total mixture energy defined as:

$$E = \rho \left(e + \frac{1}{2} u^2 \right) \tag{4}$$

where e is the mixture specific internal energy:

$$e = x_{eq} e_v + \left(1 - x_{eq}\right) e_l \tag{5}$$

x_{eq} is the equilibrium vapour quality, and ρ is the mixture density defined as:

$$\frac{1}{\rho} = \frac{x_{eq}}{\rho_v} + \frac{\left(1 - x_{eq}\right)}{\rho_l} \tag{6}$$

In Eqs. (5) and (6) the subscripts v and l refer to the vapour and liquid phases respectively.

To solve Eqs. (1)–(3) numerically, a finite volume method is used (Leveque, 2002), where, following Brown et al. (2015b), the conservative left-hand-side of Eqs. (1)–(3) are solved using the AUSM-+ flux vector splitting scheme (Liou, 2006).

2.2. Interpolation technique

As described previously, the coupling of the EoS described in Section 2.3 with the flow Eqs. (1)–(3) where the fluid is two-phase is complicated by the fact that the free variables are the density, ρ, and internal energy, e, with which we must compute the system P and temperature, T, while the computation of the phase equilibria using an EoS (in this case PC-SAFT as described in Section 2.3) is most commonly performed using the P and T of a mixture for a fixed given total composition. To overcome this, we introduce the construction of two interpolant grids, one of which is constructed using the P and T as free variables, denoted $\{P, T\}$, and the other

using ρ and e, denoted by $\{\rho, e\}$. For the composition in question, these two pairs of variables correspond to different state functions, i.e. the P and T are the state variables of the specific Gibbs energy while the ρ and e are the state variables of the specific entropy. Consequently, by definition, a one-to-one and onto map exists between the considered grids which provide the means for rapidly computing the thermodynamic properties and phase equilibria during flow simulations.

The construction begins by defining the bounds of the $\{P, T\}$ grid using the fluid conditions required for the simulation (i.e. the intervals $[T_{min}, T_{max}]$ and $[P_{min}, P_{max}]$). Grid points are sampled along isotherms which are uniformly distributed within the temperature range. Typically, for the pressure ranges of interest for CO_2 pipeline decompression, the isotherms will intersect the dew and bubble point and hence pass through the phase envelope. As a result, an interpolant has to be developed which can resolve the abrupt changes of the fluid properties with pressure and temperature within the phase coexistence regions, and in particular near the equilibrium lines. In practice this means that the points selected for building the interpolant cannot be uniformly distributed along the isotherm, but must be chosen so as to resolve the region around, and within, the phase envelope of the mixture, which is known *a priori* given the composition of the fluid.

In order to address this problem and improve the mapping, we adopt a non-uniform sampling along each isotherm, resulting in an increased density of points close to the dew and bubble point pressures (P_d and P_b respectively) and within the phase envelop itself. The set of N points along each isotherm are selected as follows:

a. if $P_{max} \leq P_d$ or $P_b \leq P_{min}$, i.e. a permanently single-phase fluid, the points are uniformly distributed in $[P_{min}, P_{max}]$:

$$P_i = P_{min} + (i-1)\frac{P_{max} - P_{min}}{N-1}, i = 1, \ldots, N \qquad (7)$$

b. if $P_{min} \leq P_d \leq P_b \leq P_{max}$, i.e. the interval $[P_{min}, P_{max}]$ encompasses the two-phase region, N_d points are distributed in $[P_{min}, P_d - \Delta]$ to increase the point density close to the dew point using:

$$P_i = P_{min} + (P_d - \Delta - P_{min})g\left(\frac{i-1}{N_d}\right), i = 1, \ldots, N_d \qquad (8)$$

N_b points are distributed uniform in $[P_b + \Delta, P_{max}]$ to increase the point density close to the bubble point using:

$$P_i = (P_b + \Delta - P_{min}) + (P_{max} - P_b - \Delta)g\left(\frac{i-1}{N_b}\right), i = 1, \ldots, N_b \quad (9)$$

while the remaining N_{VLE} points are distributed using the mapping function which increases the points density near the dew and the bubble line:

$$P_i = (P_d - \Delta) + (P_b - P_d + 2\Delta)g\left(\frac{i-1}{N_{VLE}}\right), i = 1, \ldots, N_{VLE} \qquad (10)$$

with:

$$g(x) = \frac{1 + erf(Ax - B)}{2} \qquad (11)$$

if $P_{min} \leq P_d \leq P_{max} \leq P_b$ or $P_d \leq P_{min} \leq P_b \leq P_{max}$, i.e. the interval $[P_{min}, P_{max}]$ contains part of the two-phase region a variant of the points distribution described in case b is applied. For example if $P_{min} \leq P_d \leq P_{max} \leq P_b$, the points are distributed according to (8) and (10), with the exception that in (10) P_{max} is taken as the upper limit rather than $P_b + \Delta$.

In case b, the most general, the number of points N_{VLE} is taken as 70% of the total number N, while N_d and N_b are each taken as 15% of N. The total number of points, N, as well as the distribution function parameters Δ, A and B are tuned to optimise grid's quality. In this study A and B were set equal to 4.4 and 2.2 respectively while the values used for N and Δ are reported in later sections.

At each of these points, using the P and T, the other thermodynamic properties are calculated (e.g. e, ρ). In other words, at these points we have established the maps $e(P, T)$ and $\rho(P, T)$. Using these same points we re-interpret the grid to give us the inverse maps $P(\rho, e)$ and $T(\rho, e)$, and hence a $\{\rho, e\}$ grid.

In order to increase the accuracy of this new grid across the ranges of densities and internal energies covered, we redistribute the points along an isotherm map $T(\rho, e)$ crossing the phase envelope. The corresponding path is expressed as a mono-parametric curve $(e(\lambda), \rho(\lambda))$ with $0 \leq \lambda \leq 1$. Eventually, the properties of interest along this curve are also expressed as functions of the same parameter i.e. $T(\lambda), P(\lambda)$. Using appropriate values of λ we resample the path to obtain more uniformly distributed points along the isotherm while the desired properties at the new point are calculated by interpolating the corresponding functions using univariate Akima splines (Akima, 1996). Finally, we resample the $\{\rho, e\}$ grid produced for each property of interest by using the bivariate Akima spline interpolation scheme (Akima, 1996) to improve its uniformity/regularity and consequently the efficiency of the interpolation.

Finally, using the established $\{\rho, e\}$ grids we decouple the thermodynamic calculations from the actual simulation of the flow, increasing not only the efficiency but also the reliability of the proposed approach.

2.3. Equation of state

In the present study in order to predict the properties of CO_2 and its mixtures, the PC-SAFT EoS presented by Diamantonis et al. (2013a) is applied, a brief description is given next. The PC-SAFT EoS is expressed as the summation of residual Helmholtz free energy terms that occur due to different types of intermolecular interactions between the various components in the system under study. The residual Helmholtz free energy, A^{res} is equal to the Helmholtz free energy minus the Helmholtz free energy of the ideal gas at given temperature and density. For a system that consists of associating chains (for example aqueous mixtures), PC-SAFT can be expressed as:

$$\frac{A^{res}(\rho, T)}{NRT} = \frac{a^{hs}}{RT} + \frac{a^{chain}}{RT} + \frac{a^{disp}}{RT} + \frac{a^{assoc}}{RT} \qquad (12)$$

where a is the Helmholtz free energy per mole, R is the universal gas constant and the superscripts "res", "hs", "chain", "disp", and "assoc" refer to residual, hard sphere, chain (hard chain reference fluid), dispersion, and association, respectively. The mathematical expressions for the individual terms may be found in Diamantonis et al. (2013b). More details on the SAFT EoS and its variants for pure components and their mixtures are given in Kontogeorgis and Folas (2010).

3. Results and discussion

3.1. Interpolation consistency analysis

Prior to its application to flow simulations the consistency of the interpolation method's predictions with those obtained with the underlying thermodynamic model must be assessed. For the subsequent analysis, two mixtures are chosen; a simple binary mixture of CO_2 and nitrogen (N_2) and a more complex quinternary mixture of hydrogen (H_2), oxygen (O_2), N_2, methane (CH_4) and CO_2 (Tests 26 and 31 respectively presented by Cosham et al., 2012). The composition of each mixture is shown in Table 1. The construction of the tables used a total of 100 isotherms along which N was taken to be 200, while Δ is set to zero. It should be noted that, due to the extended P and T conditions of the experimental data, and hence lower pressures and temperatures, produced for the binary mix-
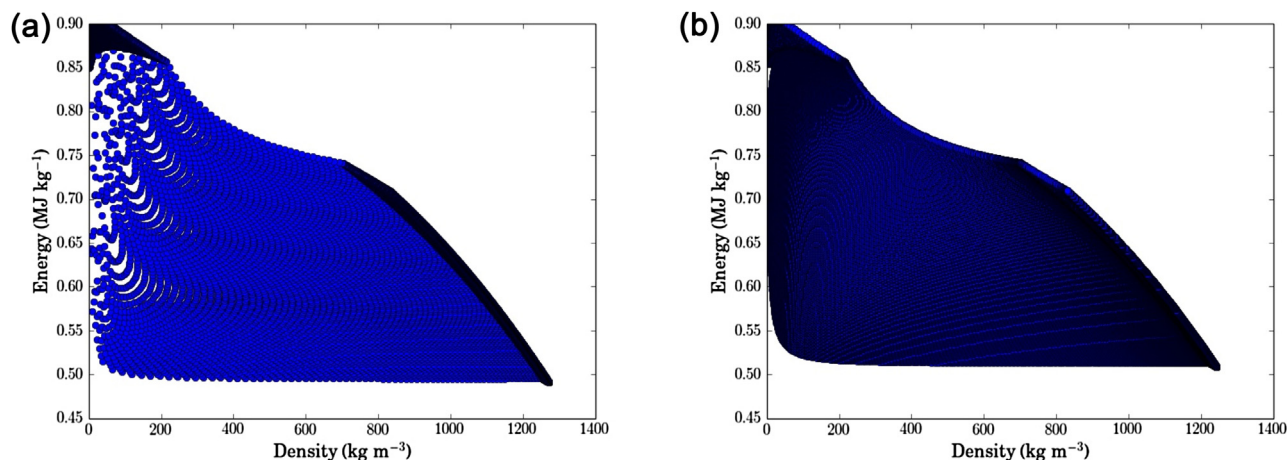
Fig. 1. The $\{\rho, e\}$ interpolation grids in the case of a uniform sampling (a) and with the adaptive sampling method (b) produced for the binary mixture of 95.96% CO_2–4.04% N_2 (vol/vol).

Table 1
Initial conditions and fluid composition for decompression experiments Test 26 and 31 (Cosham et al., 2012).

Input Parameter	Test 26	Test 31
Feed Inlet Temperature (K)	278.35	283.15
Feed Inlet Pressure (bar)	141	151.51
Fluid Composition (% vol./vol)	N_2: 4.04	H_2: 1.15
	CO_2: 95.96	N_2: 4.0
		O_2: 1.87
		CH_4: 1.95
		CO_2: 91.03

Table 2
Average absolute deviations (%) of predictions of the temperature and pressure produced by the interpolation grids.

Input Parameter	Binary	Quinternary
Temperature	0.005	0.002
Pressure	0.44	0.07

In order to quantify the deviations of the predictions obtained from the interpolation grids and the actual values calculated from the underlying EoS, 10,000 random samples are taken in the relevant $P\text{-}T$ domain. From these samples, the $e(P, T)$ and $\rho(P, T)$ functions are evaluated using the EoS and the application of the interpolation grids using these values compared with the original point. Table 2 presents the percentage average absolute deviations (% AAD) of the predictions obtained from this analysis for both the binary and quinternary mixtures. It should be noted that the grid produced from the uniform $\{P, T\}$ sampling failed to provide predictions for all of the points used in this comparison and so is omitted. As may be observed, with the exception of the binary pressure predictions for which a value of 0.44% was found, the results show an AAD% of less than 0.1%.

Fig. 3(a) and (b) shows the %AAD contours of the predicted temperature and pressure respectively, for the binary mixture. Fig. 4(a) and (b) shows the same data for the quinternary mixture. As can be seen from both Figs. 3 and 4 the error observed in the prediction of the pressure is substantially higher in places, reaching up to 10%, than for the temperature, which is less than 0.5% throughout; nevertheless, the regions of high error are restricted to low temperatures above the bubble point line which has limited physical interest. It should further be noted that this region also corresponds to conditions where solid formation may be expected, which however is not accounted for in the current thermophysical model.

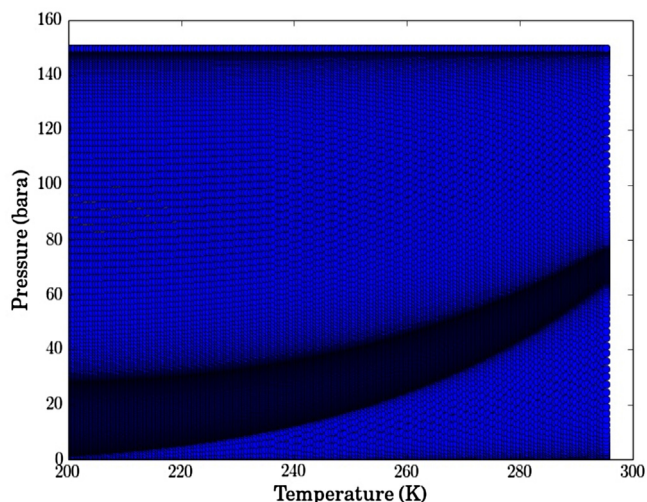**Fig. 2.** The $\{P,T\}$ interpolation grid produced with the adaptive sampling method for the binary mixture of 95.96%CO_2–4.04% N_2 (vol/vol).

3.2. Shock tube tests

In order to assess the efficacy of the interpolation technique developed in this work as a means of providing thermodynamic properties to flow simulations, two shock tube tests conducted are simulated. For the first simulation, the states are chosen such that the fluid remains in the single-phase region. For the second simulation the states are chosen to induce phase change in an initially single-phase state. The conditions for the single and two-phase shock tube tests can be found in Tables 3 and 4 respectively. In both cases, simulations are performed for both the binary and quin-
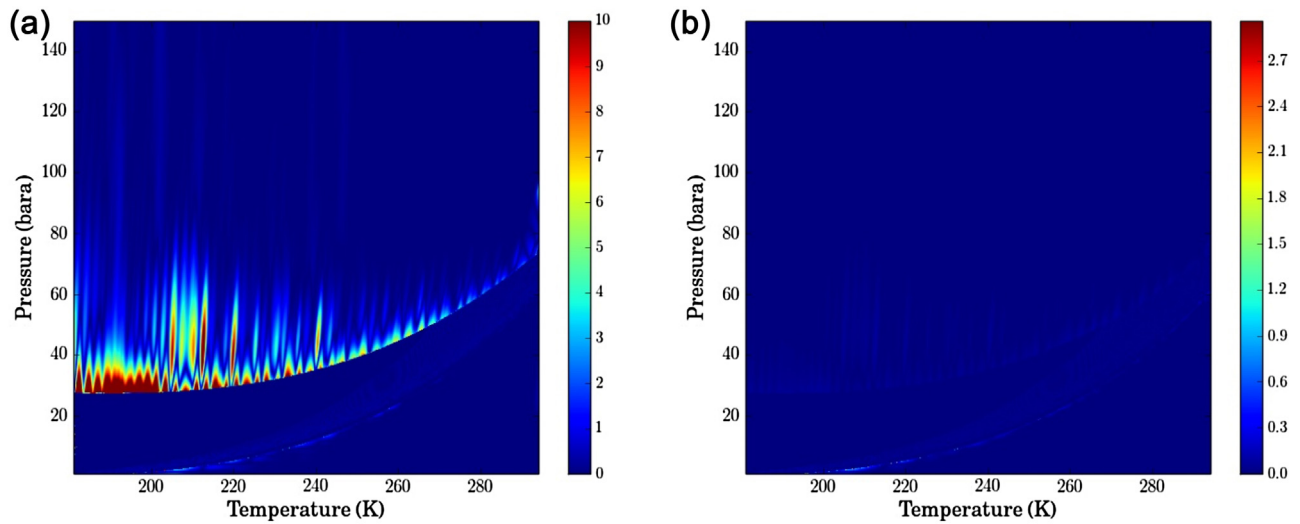
ture presented in Section 3.3, it is necessary to produce a table which extends to far lower temperatures. Fig. 1(a) and (b) respectively shows the points sampled for the $\{\rho, e\}$ constructed for the binary mixture using a uniform $\{P, T\}$ grid and using the methodology developed above. The $\{P, T\}$ grid developed for this latter is shown in Fig. 2. As can clearly be seen in Fig. 1(a) the "uniform sampling strategy" produces in a much sparser weighting of the points through the phase envelope compared to the one achieved in (b) where the re-distribution of the points results in a much greater number of samples between the dew and bubble point lines.

Fig. 3. %AAD interpolation errors observed in the pressure (a) and temperature (b) across the relevant region in the P-T phase diagram for the binary mixture.
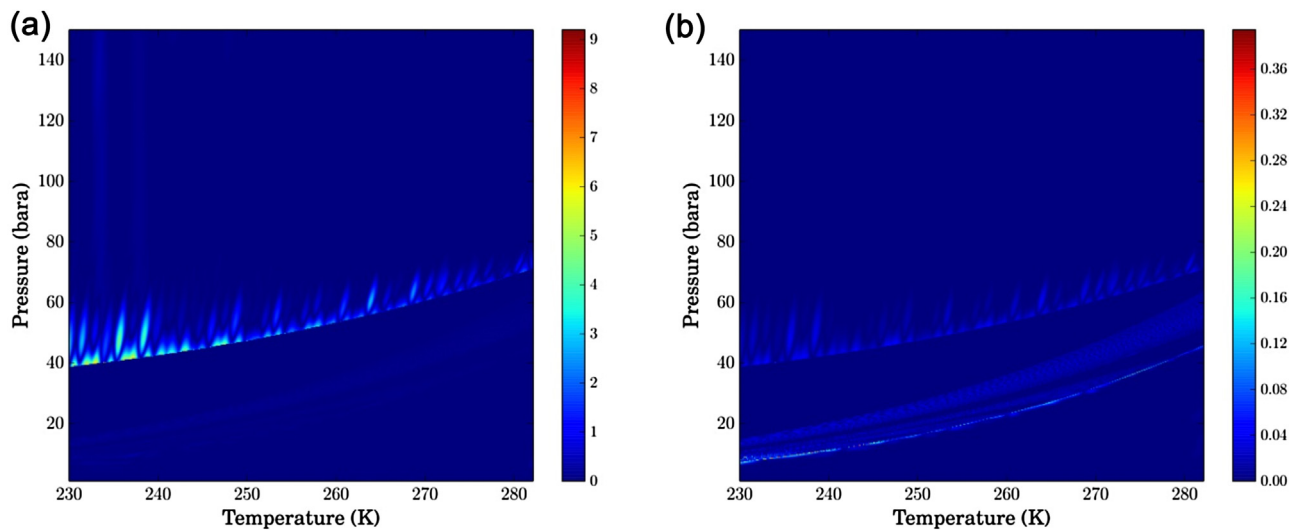

Fig. 4. %AAD interpolation errors observed in the pressure (a) and temperature (b) across the relevant region in the P-T phase diagram for the quinternary mixture.

Table 3
Initial states for the single-phase shock tube tests.

Input Parameter	P (bara)	Temperature (K)	Velocity (m s^{-1})
Left state	151	283.15	0
Right state	100	260.00	0

Table 4
Initial states for the two-phase shock tube tests.

Input Parameter	P (bara)	Temperature (K)	Velocity (m s^{-1})
Left state	151	283.15	0
Right state	P_{dew} + 2	260.00	0

ternary mixtures using a CFL number of 0.2 and 200 computational cells.

3.2.1. Single phase

Fig. 5(a)–(c) shows the profiles of the density, pressure and temperature respectively for both the binary and quinternary mixture. As may be observed from Fig. 5(a) for the density of the binary mix-

ture, an expansion wave is observed at ca. 0.3 to 0.4 separating two constant states; this is followed by a jump in the density across the discontinuity at ca. 0.6 before a smooth drop beginning at ca 0.8 and ending at ca 0.9. It is clear that the features of the results for the quinternary mixture are the same as in the binary case, with the exception that they are at a lower density level.

For the pressure (Figs. 5(b)) the results for both the binary and quinternary mixtures are almost identical; as expected the discontinuity is still present. The slight variations are likely due to the slight differences in the speed of sound and hence wave speeds. The temperature results show the same similarities between the two mixtures (Fig. 5(c)). Importantly, the interpolated results remain stable despite the presence of shock and rarefaction waves as well as contact discontinuities.

3.2.2. Two-phase

Fig. 6(a)–(d) shows the profiles of the density, vapour fraction, pressure and temperature respectively, for the binary and quinternary mixtures. While the left hand states are the same and the fluid is in the single-phase region, the state on the right is selected
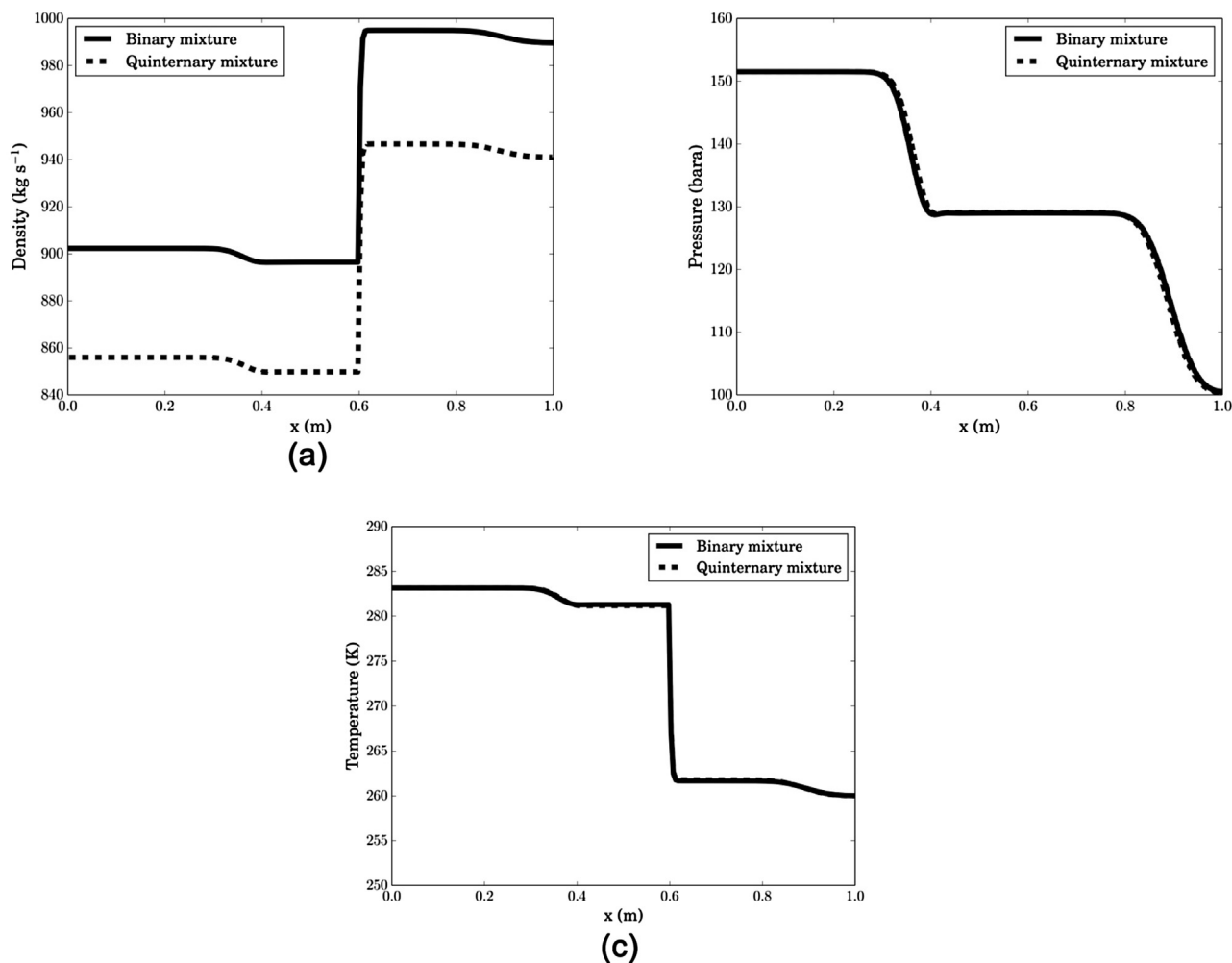
Fig. 5. Comparison of binary and quinternary mixture profiles of density (a), pressure (b) and temperature (c) for the single-phase shock tube test after 0.4 ms.

within the mixture's phase envelope. Thus, relative to the dew line, the states are different for both of the two mixtures simulated.

As Fig. 6(a) shows, for the binary mixture the density falls across the expansion wave which begins at ca. 0.3 m and ends at ca. 0.4 m. The density drops sharply at 0.58 m, where the initial boundary between the states was placed; this is followed by a slight distortion of the discontinuity at ca. 0.62 m, representing an additional wave, and a slower drop across the shock between 0.64 m and 0.68 m. Similar trends are observed for the quinternary mixture. However, the density throughout is lower and the shock wave from 0.64 m is smeared over a larger distance.

The profiles of the vapour fraction (Fig. 6(b)) shows that no vapour is produced across the expansion wave. The vapour fraction is seen to increase through the series of waves between 0.58 m and 0.64 m. Interestingly, across the shock wave, the vapour fraction increases for the binary and decreases for the quinternary mixture, which is due to the different phase equilibria through the respective mixture's phase envelopes.

Following the expansion wave, the pressures (Fig. 6(c)) obtained prior to the shockwaves is substantially higher for the quinternary mixture, and in both cases relates to the bubble line pressure of the fluids. In the case of the temperature (Fig. 6(d)), a fall is observed through the expansion wave as with the density, after this however a sharp fall is seen at discontinuity before rising and falling again. For this latter behaviour the quinternary mixture exhibits much larger changes.

3.3. Decompression tests

In the following, the robustness of the HEM outflow model coupled with the interpolation technique is evaluated for pipeline releases of CO_2 mixtures. The outflow model is validated against two sets of data obtained from Full-Bore Rupture (FBR) releases of CO_2 from a 144 m long, 150 mm internal diameter section of pipeline using the binary and quinternary mixtures introduced earlier and originally presented in Cosham et al. (2012), the data for the latter has been directly from that publication while the for the former the data presented is as yet unpublished. Table 1 presents the initial conditions and composition of fluid in the pipeline in both cases, while a complete description of the experimental setup and procedure can be found in Cosham et al. (2012). Given the very short depressurisation durations considered in both tests, heat transfer between the pipe wall and the pipe surrounding is ignored in the fluid model. The pipeline roughness was found experimentally to be 0.005 mm, while the ambient pressure was 1.01 bara.

3.3.1. Binary mixture

Fig. 7 shows comparison of the predicted and measured variation of the pressure at the closed end of the section of pipeline following the initiation of the decompression. As may be observed in the predicted results, the pressure remains initially constant but falls rapidly at ca. 0.2 s when the initial expansion wave, caused by the decompression, reaches the closed end of the pipeline. The
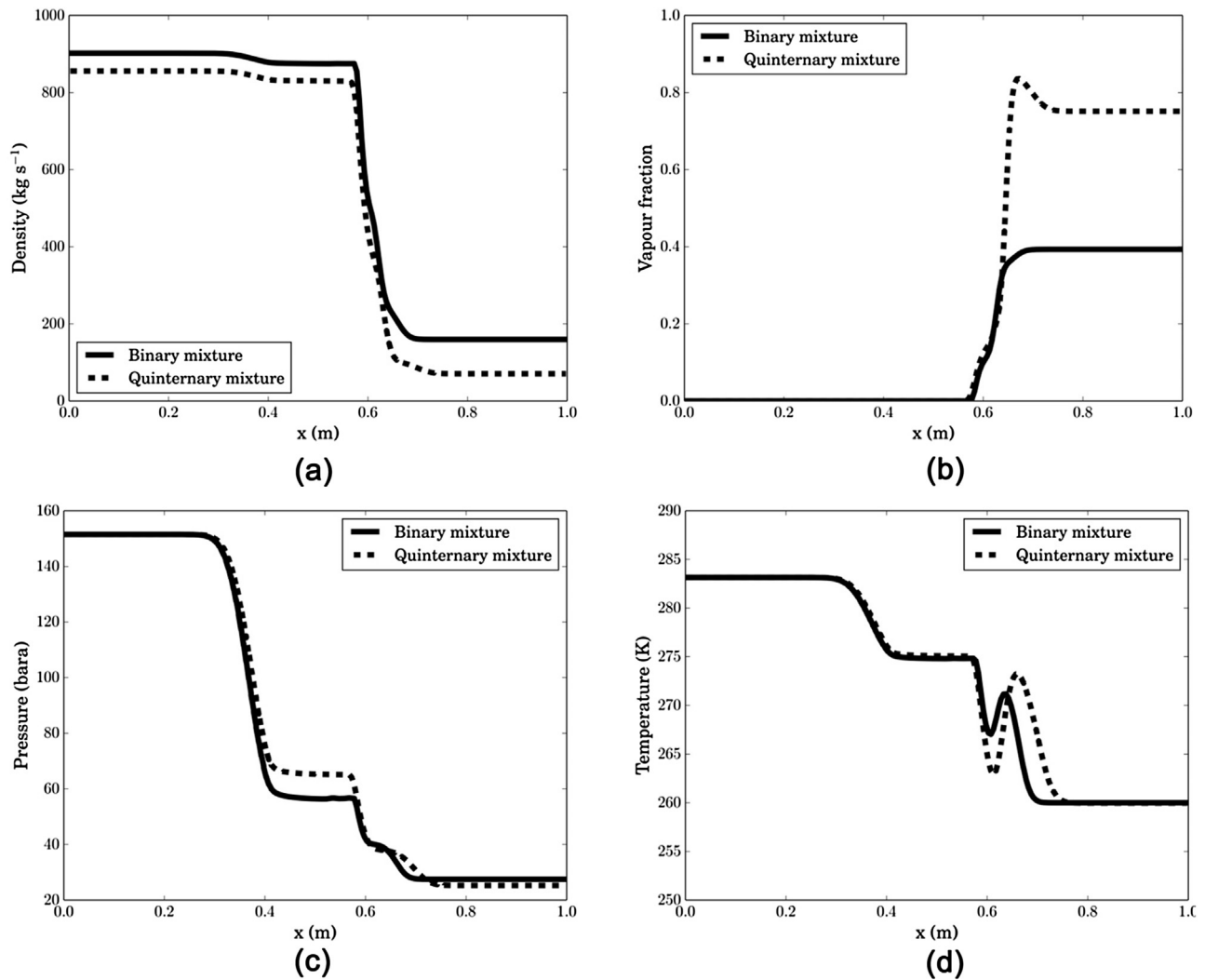
Fig. 6. Comparison of binary and quinternary mixture profiles of density (a), vapour fraction (b), pressure (c) and temperature (d) for the two-phase shock tube test after 0.4 ms.
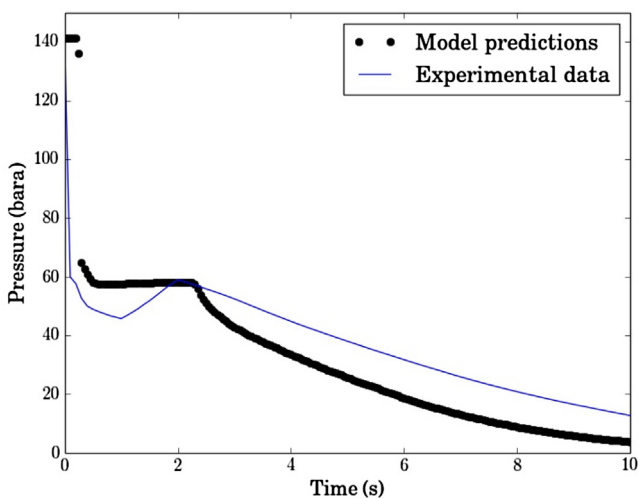

Fig. 7. Comparison of the predicted and measured variation of pressure with time at the closed end of the pipeline following the initiation of decompression.

experimental pressures shown were sampled with too low frequency to resolve this. Following this, a pressure plateau of ca. 58 bara is predicted, until ca. 2.5 s at which point the pressure begins

to fall again towards the ambient. In comparison, after the initial pressure drop, the experimental pressure is observed to fall more slowly to a minimum at ca. 1 s before recovering to a pressure very close to the plateau pressure predicted by the model. This is practically important as this pressure is that which is used in the analysis of the propagation of ductile fractures (Mahgerefteh et al., 2012a). Following this the pressure again drops, but at a slower rate than that predicted. As noted by various authors (Mahgerefteh et al., 2012b; Munkejord et al., 2010) this later behaviour is largely due to frictional and heat transfer effects, the modelling of which is outside of this study.

Fig. 8 shows the thermodynamic trajectory at the closed end of the pipeline section during the decompression relative to the dew and bubble lines. As may be observed, as noted above, during the initial decompression the fluid drops almost instantaneously along the isentrope into the phase envelope where it descends towards the dew line at low temperatures.

3.3.2. Quinternary mixture

Fig. 9 shows the comparison of the predicted pressures with the experimental data recorded at transducers P14 and P18, 1.84 m and 3.64 m from the open end of the pipeline respectively (Cosham et al., 2012). As may be observed, at both P14 and P18 the time at which the initial pressure drop occurs, 2.75 and 5.5 ms respectively,
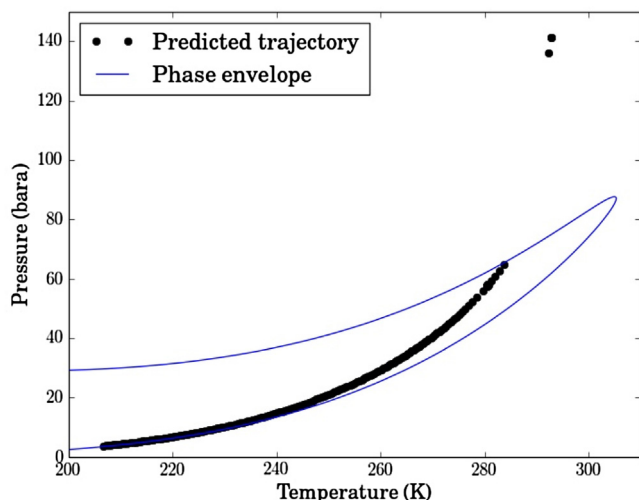
Fig. 8. Thermodynamic trajectory of the decompression relative to the binary mixture phase envelope at the closed end of the pipeline following the initiation of decompression.
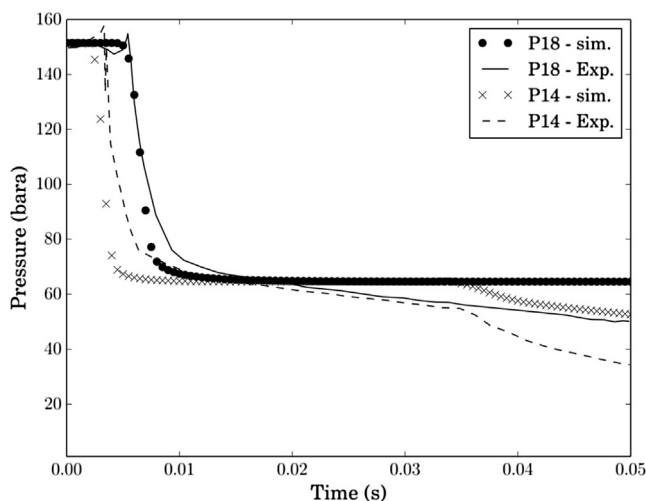

Fig. 9. Comparison of the predicted and measured variation of pressure with time 1.84 m (P14) and 3.84 (P18) from the open end of the pipeline following the initiation of decompression for the case of quinternary mixture.

is well captured. The recorded pressure during the initial decompression is seen to be slower than that predicted; this deviation can partially be explained by a lag in the measurements, given the rapidity in the pressure change.

Following this initial period of transients the simulations predict a steadying of the pressure at ca. 65 bara, at P18 this lasts for the duration of the simulation while for P14 the pressure begins to fall at ca. 36 ms. In contrast, the measured data fall steadily throughout this period, this is likely in part due to the effects of friction and heat transfer which the fluid model applied here does not capture accurately (Mahgerefteh et al., 2012b). Notably the measured pressure at P14 indicates a subsequent acceleration of the pressure drop at the time predicted by the fluid model.

4. Conclusions

This paper presents the development and application of a robust interpolation technique for the prediction of thermodynamic properties and phase equilibria of complex mixtures. The accuracy and computational burden of computing these physical proper-

ties greatly affects the overall accuracy and computational cost of multiphase multicomponent simulations. Thus, the adaption of this technique has a tremendous impact on our ability to perform sophisticated computational fluids dynamics (CFD) simulations at reasonable cost without significant loss of accuracy. Furthermore, in this work, the higher order PC-SAFT EoS was used for the accurate calculation of physical properties, to the author's knowledge it is the first attempt to use PC-SAFT for dynamic, compressible, multiphase fluid flow simulations.

The assessment of the technique's ability to reproduce the results of the EoS showed, for the most part, an error no greater than 0.5% compared to the actual EoS predictions. Large errors were observed only for the liquid phase at low temperatures, where the physical model represented by the EoS is itself not applicable, as solid formation not predicted by the EoS is expected. The extension of the current interpolation technique to a thermophysical model where the solid phase is accounted for is part of ongoing work.

Following this, the method was coupled with a fluid model and was used for the simulation of CO_2 rich mixtures, which is of particular interest in the development of CCS technology. Analysis of several hypothetical shock tube tests, as well as the comparison of the predictions against experimental decompression data, showed that the interpolation method produced robust and highly reliable results for simple and complex mixtures.

Interestingly, comparison between model predictions and experimental decompression results showed that the implementation of the interpolation technique produced a reasonable prediction of the initial depressurisation period. On-going work by the authors focuses on the development of appropriate models for the heat transfer and frictional effects to improve the accuracy of the predictions beyond this period.

Acknowledgements

References

Akima, H., 1996. Algorithm 761: Scattered-data surface fitting that has the accuracy of a cubic polynomial. ACM Trans. Math Softw. 22, 365–371.

Andresen, T., 2009. Mathematical Modeling of CO2 Based Heat Pumping Systems PhD Thesis. NTNU.

Blinkov, V., Jones, O., Nigmatulin, B., 1993. Nucleation and flashing in nozzles—2: comparison with experiments using a five-equation model for vapor void development. Int. J. Multiphase Flow 19, 965–986.

Brown, S., Beck, J., Mahgerefteh, H., Fraga, E.S., 2013. Global sensitivity analysis of the impact of impurities on CO_2 pipeline failure. Reliab. Eng. Syst. Saf. 115, 43–54, http://dx.doi.org/10.1016/j.ress.2013.02.006.

Brown, S., Fraga, E.S., Mahgerefteh, H., Martynov, S., 2015a. A geometrically based grid refinement technique for multiphase flows. Comput. Chem. Eng. 82, 25–33, http://dx.doi.org/10.1016/j.compchemeng.2015.05.031.

Brown, S., Martynov, S., Mahgerefteh, H., 2015b. Simulation of two-phase flow through ducts with discontinuous cross-section. Comput. Fluids 120, 46–56, http://dx.doi.org/10.1016/j.compfluid.2015.07.018.

Castier, M., 2009. Solution of the isochoric-isoenergetic flash problem by direct entropy maximization. Fluid Phase Equilib. 276, 7–17, http://dx.doi.org/10.1016/j.fluid.2008.10.005.

Chen, N.H., 1979. An explicit equation for friction factor in pipe. Ind. Eng. Chem. Fundam. 18, 296–297, http://dx.doi.org/10.1021/i160071a019.

Cosham, A., Jones, D.G., Armstrong, K., Allason, D., Barnett, J., 2012. The decompression behaviour of carbon dioxide in the dense phase. In: Proceedings of The 9th International Pipeline Conference, Asme, p. 447, http://dx.doi.org/10.1115/ipc2012-90461.

Diamantonis, N.I., Economou, I.G., 2011. Evaluation of statistical associating fluid theory (SAFT) and perturbed chain-SAFT equations of state for the calculation of thermodynamic derivative properties of fluids related to carbon capture and sequestration. Energy Fuels 25, 3334–3343, http://dx.doi.org/10.1021/ef200387p.

Diamantonis, N.I., Boulougouris, G.C., Mansoor, E., Tsangaris, D.M., Economou, I.G., 2013a. Evaluation of cubic, SAFT, and PC-SAFT equations of state for the

vapor-Liquid equilibrium modeling of CO2 mixtures with other gases. Ind. Eng. Chem. Res. 52, 3933–3942, http://dx.doi.org/10.1021/ie303248q.

Diamantonis, N.I., Boulougouris, G.C., Tsangaris, D.M., Kadi, M.J., El Saadawi, H., Negahban, S., Economou, I.G., 2013b. Thermodynamic and transport property models for carbon capture and sequestration (CCS) processes with emphasis on CO2 transport. Chem. Eng. Res. Des. 91, 1793–1806, http://dx.doi.org/10.1016/j.cherd.2013.06.017.

Dumbser, M., Iben, U., Munz, C.D., 2013. Efficient implementation of high order unstructured WENO schemes for cavitating flows. Comput. Fluids 86, 141–168, http://dx.doi.org/10.1016/j.compfluid.2013.07.011.

Gross, J., Sadowski, G., 2001. Perturbed-chain SAFT: an equation of state based on a perturbation theory for chain molecules. Ind. Eng. Chem. Res. 40, 1244–1260, http://dx.doi.org/10.1021/ie0003887.

Iranshahr, A., Voskov, D., Tchelepi, H.A., 2010. Generalized negative-flash method for multiphase multicomponent systems. Fluid Phase Equilib. 299, 272–284, http://dx.doi.org/10.1016/j.fluid.2010.09.022.

Kontogeorgis, G.M., Folas, G.K., 2010. Thermodynamic Models for Industrial Applications: From Classical and Advanced Mixing Rules to Association Theories. Wiley.

Leveque, R.J., 2002. Finite Volume Methods for Hyperbolic Problems Cambridge. University Press Cambridge.

Liou, M., 2006. A sequel to AUSM, part II: AUSM+-up for all speeds. J. Comput. Phys. 214, 137–170, http://dx.doi.org/10.1016/j.jcp.2005.09.020.

Mahgerefteh, H., Oke, a, Rykov, Y., 2006. Efficient numerical solution for highly transient flows. Chem. Eng. Sci. 61, 5049–5056, http://dx.doi.org/10.1016/j.ces.2006.03.012.

Mahgerefteh, H., Brown, S., Denton, G., 2012a. Modelling the impact of stream impurities on ductile fractures in CO2 pipelines. Chem. Eng. Sci. 74, 200–210, http://dx.doi.org/10.1016/j.ces.2012.02.037.

Mahgerefteh, H., Brown, S., Martynov, S., 2012b. A study of the effects of friction, heat transfer, and stream impurities on the decompression behavior in CO2 pipelines. Gases Sci. 379, 369–379, http://dx.doi.org/10.1002/ghg.

Martynov, S.B., Mason, D.J., Heikal, M.R., 2006. Numerical simulation of cavitation flows based on their hydrodynamic similarity. Int. J. Engine Res. 7, 283–296, http://dx.doi.org/10.1243/14680874JER04105.

Michelsen, M., 1982a. The isothermal flash problem. part II. phase-split calculation. Fluid Phase Equilib. 9, 21–40, http://dx.doi.org/10.1016/0378-3812(82)85002-4.

Michelsen, M.L., 1982b. The isothermal flash problem. part I. stability. Fluid Phase Equilib. 9, 1–19.

Michelsen, M.L., 1999. State function based flash specifications. Fluid Phase Equilib. 158–160, 617–626, http://dx.doi.org/10.1016/S0378-3812(99)00092-8.

Mohebbinia, S., 2013. Advanced Equation of State Modeling for Compositional Simulation of Gas Floods. University of Texas.

Munkejord, S.T., Hammer, M., 2015. Depressurization of CO2-rich mixtures in pipes: two-phase flow modelling and comparison with experiments. Int. J. Greenhouse Gas Control 37, 398–411, http://dx.doi.org/10.1016/j.ijggc.2015.03.029.

Munkejord, S.T., Jakobsen, J.P., Austegard, A., Mølnvik, M.J., 2010. Thermo- and fluid-dynamical modelling of two-phase multi-component carbon dioxide mixtures. Int. J. Greenhouse Gas Control 4, 589–596, http://dx.doi.org/10.1016/j.ijggc.2010.02.003.

Porter, R.T.J., Fairweather, M., Pourkashanian, M., Woolley, R.M., 2015. The range and level of impurities in CO2 streams from different carbon capture sources. Int. J. Greenhouse Gas Control 36, 161–174, http://dx.doi.org/10.1016/j.ijggc.2015.02.016.

Saha, S., Carroll, J.J., 1997. The isoenergetic-isochoric flash. Fluid Phase Equilib. 138, 23–41, http://dx.doi.org/10.1016/S0378-3812(97)00151-9.

Simões-Moreira, J., Bullard, C., 2003. Pressure drop and flashing mechanisms in refrigerant expansion devices. Int. J. Refrig. 26, 840–848, http://dx.doi.org/10.1016/S0140-7007(03)00070-7.

Span, R., Wagner, W., 1996. A new equation of state for carbon dioxide covering the fluid region from the triple-point temperature to 1100 K at pressures up to 800 MPa. J. Phys. Chem. Ref. Data, 25.

Yan, W., Varzandeh, F., Stenby, E.H., 2015. PVT modeling of reservoir fluids using PC-SAFT EoS and Soave-BWR EoS. Fluid Phase Equilib. 386, 96–124, http://dx.doi.org/10.1016/j.fluid.2014.11.022.

Zaydullin, R., Voskov, D.V., James, S.C., Henley, H., Lucia, A., 2014. Fully compositional and thermal reservoir simulation. Comput. Chem. Eng. 63, 51–65, http://dx.doi.org/10.1016/j.compchemeng.2013.12.008.

Zucrow, M.J., Hoffman, J.D., 1975. Gas Dynamics. Wiley, New York.